The 8th European Congress on Computational Methods in Applied Sciences and Engineering
ECCOMAS Congress 2022
5–9 June 2022, Oslo, Norway

MODAL ANALYSIS OF A 3D GRAVITATIONAL LIQUID SHEET

A. COLANERA[1], A. DELLA PIA[1], M. R. ACQUAVIVA[1], M. CHIATTO[1] AND L. DE LUCA[1]

[1] Department of Industrial Engineering (DII)
Universitá degli studi di Napoli ”Federico II”
p.le Tecchio 80, 80125, Naples, Italy
e-mail: antonio.colanera@unina.it

Key words: Multiphase flows, Reduced Order Modeling, Modal Analysis

Abstract. Modal analysis of three-dimensional gravitational thin liquid sheet flows, interacting with unconfined gaseous environments located on both sides of the liquid phase, is performed in the present work. Numerical data of this relevant two-phase flow configuration are obtained through the single-phase formulation and the Volume-of-Fluid (VOF) technique implemented in the flow solver Basilisk. This class of flows exhibits a variety of spatial and temporal relevant structures, both in free and forced configurations, that are investigated through the Spectral Proper Orthogonal Decomposition (SPOD). By means of such methodology, we explore the effect of two main governing parameters on the flow dynamics, namely the liquid sheet aspect ratio, $AR = W/H$, where H and W are the sheet inlet thickness and width, and the Weber number, $We = \rho_l U^2 H/(2\sigma)$, in which U is the inlet liquid velocity, ρ_l the liquid density, and σ the surface tension coefficient. Finally, for the highest aspect ratio value considered ($AR = 40$), we investigate the forced dynamics of the system excited by a harmonic perturbation in transverse velocity component applied at the inlet section, comparing results with ones arising from a purely two-dimensional analysis of the flow. The obtained results highlight the low rank behavior exhibited by the flow, suggesting that reduced order modeling could be particularly appealing to reduce complexity and computational effort in numerical simulation of this class of flows.

1 INTRODUCTION

Vertical liquid jets (sheet or curtain flows) are an interesting industrial class of flows, whose modeling has been investigated since the middle of the last century. Liquid sheet flows are employed in a great variety of technological sectors, such as fuel atomization [1], paper making [2]. and coating processes [3].

Nowadays, several aspects of the unsteady dynamics of liquid curtains are a matter of active research [4], [5] and [6].

An open problem regarding this class of flows is the physical mechanism leading to the increase of dominant frequency and the sheet break-up when the inlet flow rate is reduced. On the other hand, the destabilizing role of the surface tension has been well established, see [7], [8], [9], [10] and [11].

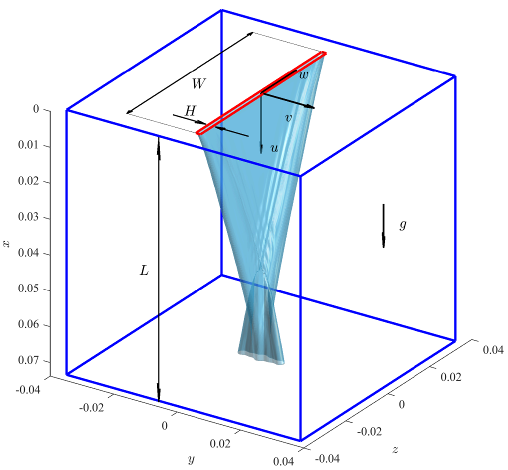

Figure 1: Main geometrical parameters of the configuration.

The comprehension of complex flows takes advantage from the recognition of physically important features which characterize the flow spatial topology and temporal evolution ([12]). In order to reduce the complexity of the underlying governing equations several low-order models based on the perturbative approach have been proposed [13], [14]. Modern data-driven modal techniques can lead to the formulation of Reduced Order Models (ROM) inheriting the main features of the Full Order Model (FOM), but requiring far lesser computational effort, [15], [16], [17].

The present work aims at performing a data-driven modal decomposition analysis of 3D gravitational liquid sheets to extract the spatial and temporal most relevant structures of this flow. Numerical data have been obtained by means of Volume-of-Fluid (VOF) based simulations. The effects of the flow rate reduction, the aspect ratio (AR) and the forcing at the inlet section on the flow topology and the spectral content are explored. A data-driven modal technique, the spectral proper orthogonal decomposition (SPOD), has been used.

2 VOLUME-OF-FLUID (VOF) SIMULATION

Numerical data of thin liquid sheet flows have been obtained through the single-phase formulation and the Volume-of-Fluid (VOF) approach [18], as shown in [19]. In Figure 1 is reported a sketch of the configuration and the main geometrical parameters.

In the VOF framework the governing equations are:

$$\frac{\partial u_i}{\partial x_i} = 0 \tag{1a}$$

$$\rho\left(\frac{\partial u_i}{\partial t} + u_j \frac{\partial u_i}{\partial x_j}\right) = -\frac{\partial p}{\partial x_i} + \rho g_i + \frac{\partial}{\partial x_j}\left[\mu\left(\frac{\partial u_i}{\partial x_j} + \frac{\partial u_j}{\partial x_i}\right)\right] + \sigma \kappa n_i \delta_S \tag{1b}$$

in which the density ρ and the viscosity μ are modelled as:

$$\rho = \rho_a + (\rho_l - \rho_a)C \tag{2a}$$

$$\mu = \mu_a + (\mu_l - \mu_a)C \tag{2b}$$

with the introduction of a new field variable, the volume fraction, C. In Eq.s (2) pedices a/l refer to ambient/liquid phase respectively. Across the interface $0 < C < 1$, otherwise $C = 0$ in the ambient phase and 1 in the liquid one. For the problem closure and to localize the interface a further equation for C is needed:

$$\frac{\partial C}{\partial t} + \frac{\partial C u_i}{\partial x_i} = 0. \tag{3}$$

The equations are solved with BASILISK code (http://basilisk.fr), see [20].

Dealing with a set of dimensionless parameters instead of dimensional quantities promotes the reproducibility of an experiment and/or of a numerical simulation and makes easier the identification of critical parameters and scaling laws. For this configuration the main governing dimensionless parameters are: the Weber number $We = \rho_l U^2 H/2\sigma$, the aspect ratio $AR = W/H$, the Froude number $Fr = U^2/gL$, the Reynolds number $Re = \rho_l U H/2\mu_l$, the sheet slenderness ratio $\varepsilon = H/L$, the density $r_\rho = \rho_a/\rho_l$ and the viscosity ratio $r_\mu = \mu_a/\mu_l$.

In this work we explored the effects of the variation of the We and AR. Our analysis focuses also on the effect of enforcing a sinusoidal boundary condition at the inlet section in transversal velocity component v:

$$v = \hat{A}U \, \sin\left(2\pi f_f (t - t_s)\right) \, \Theta\left(t - t_s\right), \tag{4}$$

in which $\hat{A}$ is a dimensionless parameter defining the oscillations amplitude, t_s is starting time of the forcing and Θ the Heaviside function. The forcing frequency f_f has been made dimensionless by introducing the Strouhal number $St_f = \dfrac{f_f H}{U}$.

3 DATA-DRIVEN MODAL ANALYSIS

In this work Spectral Proper Orthogonal Decomposition (SPOD) has been employed. The SPOD technique allows to characterize the spatial and temporal evolution of coherent structures by means of flow decomposition in various modes, each one with its own frequency, see [21] and [22].

Any field variable ϕ is decomposed as the sum of its temporal mean plus the fluctuation: $\phi(x, y, z, t) = \bar{\phi}(x, y, z) + \phi'(x, y, z, t)$. Accordingly, the state vector $\boldsymbol{q}$, in the framework of multiphase flows, is composed of u', v', w' and C' in each point of the field. To obtain the SPOD modes, flow snapshots are firstly grouped in N_b blocks $\mathbf{Q}^{(j)}$

$$\mathbf{Q}^{(j)} = \left[\mathbf{q}_1^{(j)}, \mathbf{q}_2^{(j)}, ..., \mathbf{q}_{N_f}^{(j)}\right], \tag{5}$$

then a windowed DFT is performed in each block to obtain N_b realizations of each Fourier component that are collected in N_f matrices $\hat{\mathbf{Q}}_k$. SPOD modes satisfy the eigenvalue problem of the cross-spectral density tensor $\mathbf{S}_k = \hat{\mathbf{Q}}_k \hat{\mathbf{Q}}_k^*$:

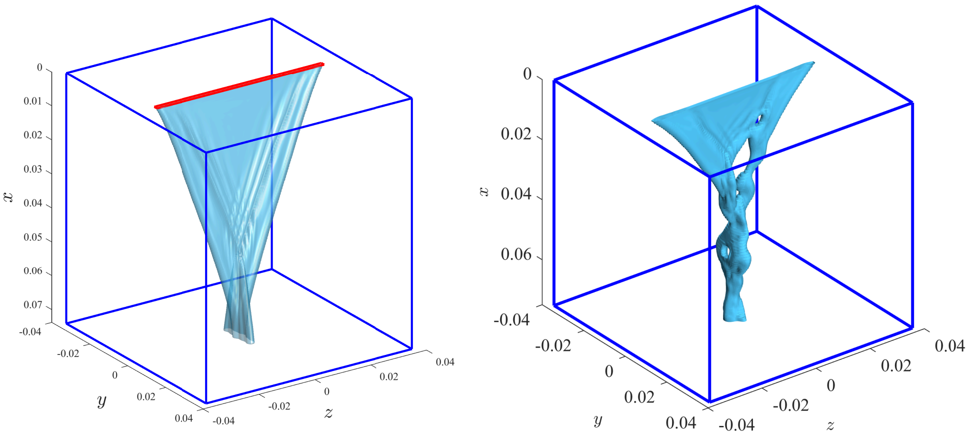

(a) $We = 2.5$ (b) $We = 0.75$

Figure 2: Snapshot of interface shape for $We = 2.5$ and 0.75, $AR = 40$.

$$\mathbf{S}_k \mathbf{W} \mathbf{\Phi}_k = \mathbf{\Phi}_k \mathbf{\Lambda}_k, \tag{6}$$

which is computed one frequency (k) at a time, to obtain modes ($\mathbf{\Phi}_k$) and eigenvalues ($\mathbf{\Lambda}_k$).

Following the work of [23], matrix $\mathbf{W}$, can be computed according to the kinetic energy of the disturbances:

$$E = \int_\Omega \left[\bar{\rho} \left(u'^2 + v'^2 + w'^2 \right) + \left(\bar{u}^2 + \bar{v}^2 + \bar{w}^2 \right) \frac{\Delta \rho^2}{\bar{\rho}} C'^2 \right] d\Omega, \tag{7}$$

where $\Delta\rho = \rho_l - \rho_a$. As shown in [24] and [25], a low-rank reconstruction of the fluctuation field based on the SPOD modes ($\mathbf{\Phi}_k$) can be obtained through the inverse DFT of the Fourier realizations matrix $\hat{\boldsymbol{Q}}_k = \mathbf{\Phi}_k \mathbf{\Lambda}_k \mathbf{\Psi}_k^*$, where $\mathbf{\Psi}_k$ is the matrix containing the eigenvectors of $\hat{\boldsymbol{Q}}_k^* \hat{\boldsymbol{Q}}_k$. For a rank r reconstruction $\hat{\boldsymbol{Q}}_k$ can be approximated as:

$$\hat{\boldsymbol{Q}}_k \approx \tilde{\mathbf{\Phi}}_{\boldsymbol{k}} \tilde{\mathbf{\Lambda}}_k \tilde{\mathbf{\Psi}}_k^*, \tag{8}$$

where $\tilde{\mathbf{\Phi}}_{\boldsymbol{k}}$ and $\tilde{\mathbf{\Psi}}_k$ are, respectively, the first r columns of $\mathbf{\Phi}_k$ and $\mathbf{\Psi}_k$.

4 RESULTS

4.1 Base case

At moderately high We, the flow is stationary. In panel (a) of Figure 2 is reported a snapshot of the interface location for $We = 2.5$ and $AR = 40$. Three main regions of the flow are detected: for $0 < x/L < 0.4$ a 2D flow, for $0.4 < x/L < 0.7$ a varicose shape and for $x/L > 0.7$ the 3D rims convergence.

In subcritical regime ($We < 1$) the flow in unsteady. Panel (b) of Figure 2 contains a snapshot of the interface location for $We = 0.75$ in which it is possible to notice that the flow regime characterized by three-dimensional asymmetric holes enucleation and advection and by irregular dynamics of the columnar curtain tail.

The application of SPOD highlights some interesting features of the flow field. In panel (a) of Figure 3 is reported the SPOD spectrum for the base case analysis ($We = 0.75$). The largest modal separation occurs at $St = 0.19$ corresponding to a dimensional frequency $f \approx 34$Hz. The

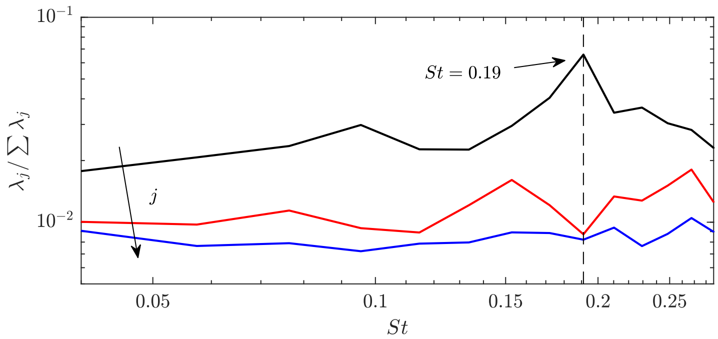

(a) SPOD spectrum

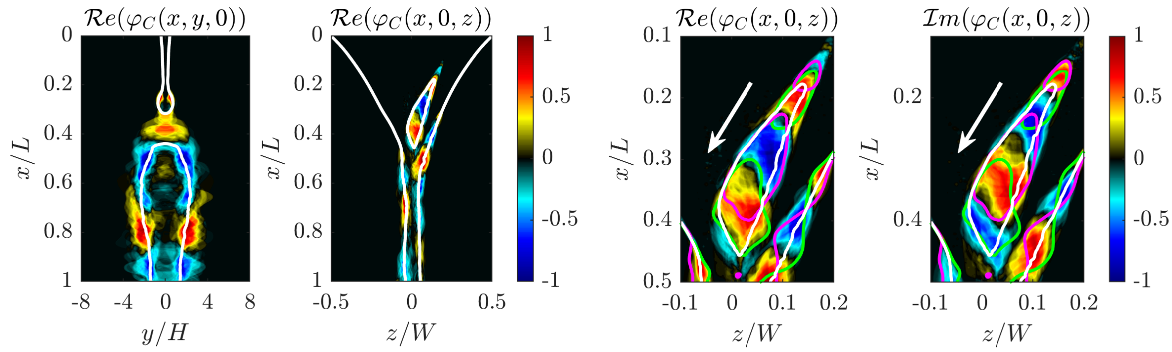

(b) C' mode (xy plane)

(c) C' mode (xz plane)

(d) Zoom of C' mode real part

(e) Zoom of C' mode imag. part

Figure 3: (a) SPOD spectrum for $We = 0.75$. SPOD parameters: $N_t = 230$, $N_b = 6$, $N_f = 64$, Hamming window for DFT, j is the running index associated with the modes. (b)-(c) Leading mode of C' in the planes xy and xz. (d)-(e) Zoom of C' leading mode (real and imaginary parts) in the holes region. The white arrows identify the advection direction.

inspection of the leading mode of C', reported in panels (b) and (c) for the principal planes xy and xz, reveals that the columnar curtain tail exhibits an irregular dynamics and, according to the definitions given in [24], it reports different symmetries in the two main planes. Panels (d) and (e) contain a zoom of C' leading mode (real and imaginary parts) in the holes region. Green and magenta lines are two snapshots of the interface location. The spatial shift of real and imaginary parts highlights the advection direction.

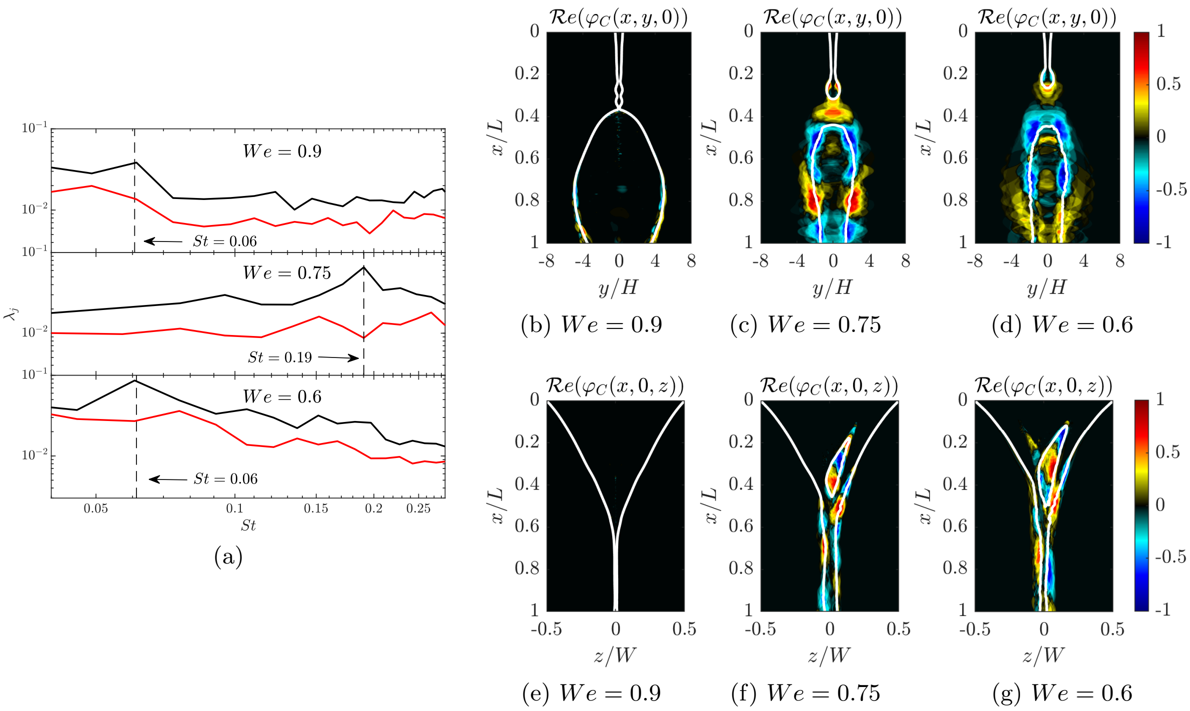

Figure 4: Effect of the Weber number We. (a) SPOD spectra at several We. SPOD parameters: $N_t = 230$, $N_b = 6$, $N_f = 64$, Hamming window for DFT, only first 2 modes are reported. (b)-(g) Leading C' mode at several We.

4.2 Effect of We

The effect of the variation of the We will be hereafter explored. We influences both the leading frequency and the spatial topology of the leading modes. By looking at SPOD spectra at several We, reported in panel (a) of Figure 4, it is possible to notice that the flow presents leading frequency at $St = 0.06$ for $We = 0.9$. Decreasing the flow rate, that correspond to a decrease of the We, the leading frequency firstly increases and then decreases again. This occurrence can be further investigated by looking at the leading modes reported in panels (b)-(g). At $We = 0.9$ the flow if slightly unsteady and the modes exhibit a shape very close to that of the supercritical configurations (panels (b) and (e)). The region with $We \approx 0.75$ is characterized by rapid holes formation and advection. With a further decrease in We, holes dimension increase and the characteristic frequency decreases.

4.3 Effect of AR

The aspect ratio does not affect the leading frequency but changes the spatial topology of the leading modes. Panel (a) of Figure 5 reveals that the variation of the aspect ratio does not influences significantly the leading St, as both configurations present a peak frequency at $St \approx 0.19$. As regards the leading modes, reported in panels (b)-(e), it is possible to notice that at the lower aspect ratio the sheet does not experiences the rupture anymore. As regards the tail region, at the higher AR the flow experiences an irregular dynamics, whereas at the lower one the motion is purely varicose.

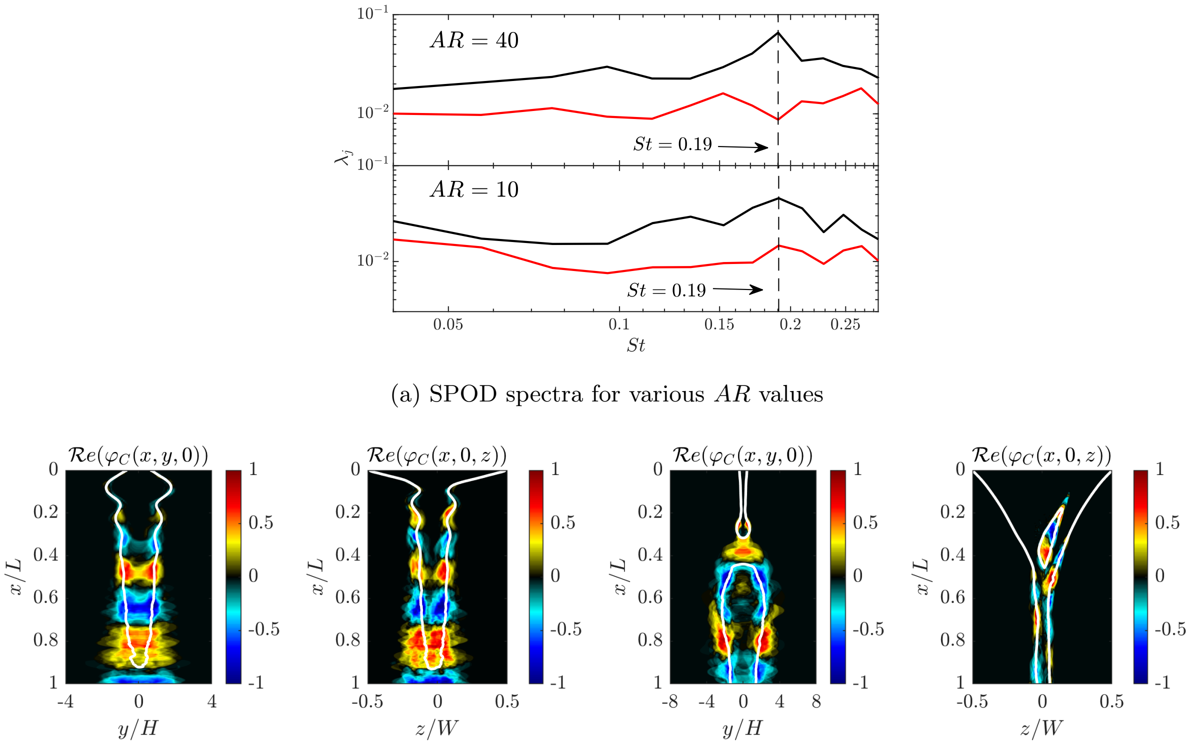

(a) SPOD spectra for various AR values

(b) $AR = 10$ (c) $AR = 10$ (d) $AR = 40$ (e) $AR = 40$

Figure 5: Effect of the aspect ratio AR. (a) SPOD spectra at several AR. (b)-(c) C' mode for $AR = 10$. (d)-(e) C' mode for $AR = 40$.

4.4 Forced configurations

In this section the effects of enforcing a sinusoidal boundary condition in the v velocity component at the inlet section are analyzed.

In Figure 6 are reported the SPOD spectrum (panel (a)) and the leading C' mode at the leading frequency in the plane xy (panel (b)) for the configuration at $We = 2.5$. The forcing frequency has been set to $f_f = 25$Hz, corresponding to a $St_f = 0.07$, and the dimensionless amplitude is $\hat{A} = 0.02$. The SPOD spectrum reports peaks at the actuation frequency and its harmonics. In this regime the flow retains the sinusoidal behavior imposed by BCs because looking at panel (b) the flow reports symmetries related to the sinusoidal perturbations ([24]).

In subcritical regime ($We = 0.75$) the sheet has a nonlinear response to the forcing. Looking at panel (a) of Figure 7 it is possible to notice that, even if the forcing St is equal to 0.14 ($f_f = 25$Hz), the leading frequency is at $St = 0.047$ that is different from both the forcing frequency ($St = 0.14$) and the leading frequency of the free system ($St = 0.19$) analyzed in previous sections. Moreover, panel (b) reveals that the mean dimension of the hole decreases in presence of the forcing.

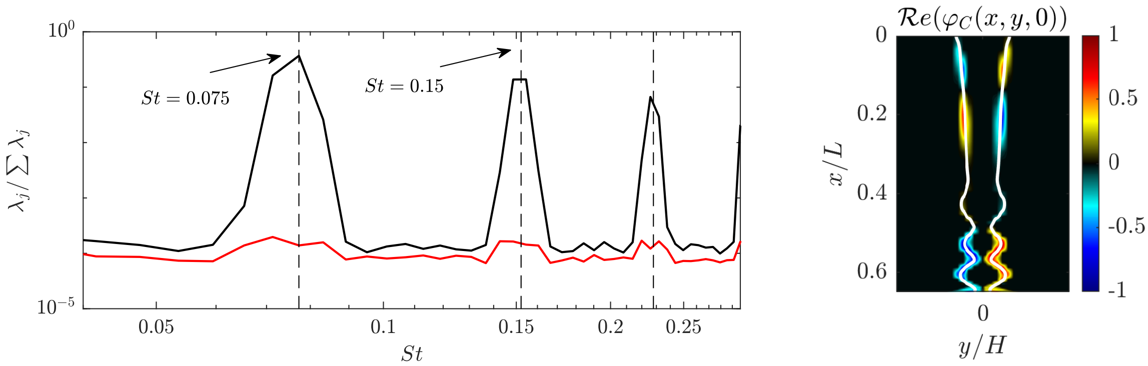

(a) SPOD spectrum (b) C' mode

Figure 6: Effect of forcing on v at the inlet section. $We = 2.5$, $AR = 40$.

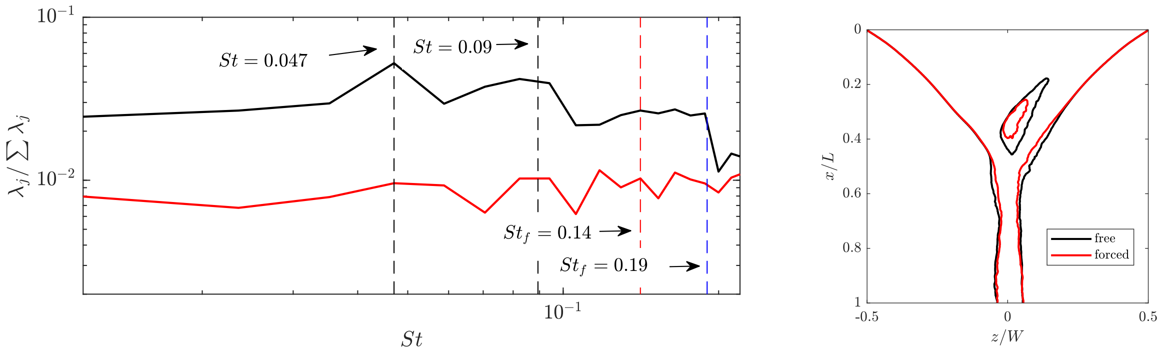

(a) SPOD spectrum (b) C' mode

Figure 7: Effect of forcing on v at the inlet section. $We = 0.75$, $AR = 40$.

5 CONCLUSIONS

A data-driven modal analysis of 3D gravitational liquid sheet direct numerical simulations has been carried out. SPOD technique has been employed for the identification of the leading spatial and temporal structures of the flow.

The analysis highlighted the nucleation of three-dimensional asymmetric holes and their advection, characterizing the topology of the liquid sheet at low flow rate. The effects of the Weber number variation have been analyzed. It has been found that the leading frequency presents a maximum in the region around $We \approx 0.75$ that is characterized by rapid holes formation and advection.

The aspect ratio (AR) does not affect the leading frequency but changes the flow topology. At high AR there is a combined sinuous/varicose behavior of the sheet whereas at low AR the evolution is purely varicose.

The imposition of harmonic forcing at the inlet section in transverse velocity v reveal the strong nonlinear behavior of the curtain at low We.

The obtained results highlight the low rank behavior exhibited by the flow, suggesting that reduced order modeling could be particularly appealing to reduce complexity and computational effort in numerical simulation of two-phase flows.

References

[1] A.H. Lefebvre and V.G. McDonell. *Atomization and Sprays.* CRC Press, 2017.

[2] Fredrik Lundell, L. Daniel Söderberg, and P. Henrik Alfredsson. Fluid mechanics of papermaking. *Annual Review of Fluid Mechanics*, 43:195 – 217, 2011.

[3] S.J. Weinstein and K.J. Ruschak. Coating flows. *Annual Review of Fluid Mechanics*, 36:29–53, 2004.

[4] S. J. Weinstein, D. S. Ross, K. J. Ruschak, and N. S. Barlow. On oblique liquid curtains. *Journal of Fluid Mechanics*, 876:R3, 2019.

[5] A. Della Pia, M. Chiatto, and L. de Luca. Receptivity to forcing disturbances in subcritical liquid sheet flows. *Physics of Fluids*, 33:032113, 2021.

[6] A. Della Pia, M. Chiatto, and L. de Luca. Global eigenmodes of thin liquid sheets by means of Volume-of-Fluid simulations. *Physics of Fluids*, 32:082112, 2020.

[7] L. de Luca and C. Meola. Surfactant effects on the dynamics of a thin liquid sheet. *Journal of Fluid Mechanics*, 300:71–85, 1995.

[8] L. de Luca. Experimental investigation of the global instability of plane sheet flows. *Journal of Fluid Mechanics*, 399:355–376, 1999.

[9] G. Coppola, F. De Rosa, and L. de Luca. Surface tension effects on the motion of a free-falling liquid sheet. *Physics of Fluids*, 25(6):062103, 2013.

[10] L. de Luca and M. Costa. Instability of a spatially developing liquid sheet. *Journal of Fluid Mechanics*, 331:127–144, 1997.

[11] A. Della Pia, A. Colanera, and M. Chiatto. Surface tension-induced instability in spatially developing subcritical liquid curtains. *Physics of Fluids*, 34:042122, 2022.

[12] C. W. Rowley and S. T.M. Dawson. Model reduction for flow analysis and control. *Annual Review of Fluid Mechanics*, 49(1):387–417, 2017.

[13] M. Girfoglio, F. De Rosa, G. Coppola, and L. de Luca. Unsteady critical liquid sheet flows. *Journal of Fluid Mechanics*, 821:219–247, 2017.

[14] F. De Rosa, M. Girfoglio, and L. de Luca. Global dynamics analysis of nappe oscillation. *Physics of Fluids*, 26(12):122109, 2014.

[15] K. Carlberg, Y. Choi, and S. Sargsyan. Conservative model reduction for finite-volume models. *Journal of Computational Physics*, 371:280–314, 2018.

[16] G. Stabile and G. Rozza. Finite volume pod-galerkin stabilised reduced order methods for the parametrised incompressible navier–stokes equations. *Computers & Fluids*, 173:273–284, 2018.

[17] B. Sanderse. Non-linearly stable reduced-order models for incompressible flow with energy-conserving finite volume methods. *Journal of Computational Physics*, 421:109736, 2020.

[18] C. W. Hirt and B. D. Nichols. Volume of fluid (VOF) method for the dynamics of free boundaries. *Journal of Computational Physics*, 39(1):201–225, 1981.

[19] R. Scardovelli and S. Zaleski. Direct numerical simulation of free-surface and interfacial flow. *Annual Review of Fluid Mechanics*, 31(1):567–603, 1999.

[20] S. Popinet. An accurate adaptive solver for surface-tension-driven interfacial flows. *Journal of Computational Physics*, 228(16):5838–5866, 2009.

[21] A. Towne, O. T. Schmidt, and T. Colonius. Spectral proper orthogonal decomposition and its relationship to dynamic mode decomposition and resolvent analysis. *Journal of Fluid Mechanics*, 847:821–867, 2018.

[22] O. T. Schmidt and T. Colonius. Guide to spectral proper orthogonal decomposition. *AIAA Journal*, 58(3):1023–1033, 2020.

[23] A. Della Pia, A. Colanera, M. Chiatto, and L. de Luca. Energy insights into the unsteady dynamics of a viscous gravitational liquid sheet. *Physics of Fluids*, 33:092118, 2021.

[24] A. Colanera, A. Della Pia, M. Chiatto, L. de Luca, and F. Grasso. Modal decomposition analysis of unsteady viscous liquid sheet flows. *Physics of Fluids*, 33(9):092117, 2021.

[25] M. Chiatto, L. de Luca, and F. Grasso. Modal analysis of actively controlled flow past a backward facing ramp. *Physical review fluids*, 6:064608, 2021.